

---

# Pegylated Arg-Gly-Asp Peptide: $^{64}\text{Cu}$ Labeling and PET Imaging of Brain Tumor $\alpha_v\beta_3$ -Integrin Expression

Xiaoyuan Chen, PhD<sup>1</sup>; Yingping Hou, MD<sup>1</sup>; Michel Tohme, MS<sup>1</sup>; Ryan Park, BS<sup>1</sup>; Vazgen Khankaldyyan, BS<sup>2</sup>; Ignacio Gonzales-Gomez, MD<sup>2</sup>; James R. Bading, PhD<sup>1</sup>; Walter E. Laug, MD<sup>2</sup>; and Peter S. Conti, MD, PhD<sup>1</sup>

<sup>1</sup>PET Imaging Science Center, Keck School of Medicine, University of Southern California, Los Angeles, California; and <sup>2</sup>Department of Pediatrics, Children's Hospital Los Angeles, Los Angeles, California

The  $\alpha_v$ -integrins, cell adhesion molecules that are highly expressed on activated endothelial cells and tumor cells but not on dormant endothelial cells or normal cells, present an attractive target for tumor imaging and therapy. We previously coupled a cyclic Arg-Gly-Asp (RGD) peptide, c(RGDyK), with 1,4,7,10-tetraazacyclododecane-*N,N',N'',N'''*-tetraacetic acid (DOTA) and labeled the RGD-DOTA conjugate with  $^{64}\text{Cu}$  (half-life, 12.8 h; 19%  $\beta^+$ ) for solid tumor targeting, with high tumor-to-background contrast. The rapid tumor washout rate and persistent liver and kidney retention of this tracer prompted us to optimize the tracer for improved pharmacokinetic behavior. In this study, we introduced a polyethylene glycol (PEG; molecular weight, 3,400) moiety between DOTA and RGD and evaluated the  $^{64}\text{Cu}$ -DOTA-PEG-RGD tracer for microPET imaging in brain tumor models. **Methods:** DOTA was activated in situ and conjugated with RGD-PEG-NH<sub>2</sub> under slightly basic conditions.  $\alpha_v\beta_3$ -Integrin-binding affinity was evaluated with a solid-phase receptor-binding assay in the presence of [<sup>125</sup>I]-echistatin. Female nude mice bearing subcutaneous U87MG glioblastoma xenografts were administered  $^{64}\text{Cu}$ -DOTA-PEG-RGD, and the biodistributions of the radiotracer were evaluated from 30 min to 4 h after injection. microPET (20 min of static imaging at 1 h after injection) and then quantitative autoradiography were used for tumor visualization and quantification. The same tracer was also applied to an orthotopic U87MG model for tumor detection. **Results:** The radiotracer was synthesized with a high specific activity (14,800–29,600 GBq/mmol [400–800 Ci/mmol]). The c(RGDyK)-PEG-DOTA ligand showed intermediate binding affinity for  $\alpha_v\beta_3$ -integrin (50% inhibitory concentration,  $67.5 \pm 7.8$  nmol/L [mean  $\pm$  SD]). The pegylated RGD peptide demonstrated rapid blood clearance ( $0.57 \pm 0.15$  percentage injected dose [%ID]/g [mean  $\pm$  SD] at 30 min after injection and  $0.03 \pm 0.02$  %ID/g at 4 h after injection). Activity accumulation in the tumor was rapid and high at early time points ( $2.74 \pm 0.45$  %ID/g at 30 min after injection), and some activity washout was seen over time ( $1.62 \pm 0.18$  %ID/g at 4 h after injection). Compared with  $^{64}\text{Cu}$ -DOTA-RGD, this tracer showed improved in vivo kinetics, with significantly reduced liver uptake ( $0.99 \pm 0.08$  %ID/g vs.  $1.73 \pm 0.39$  %ID/g at 30 min after injection and

$0.58 \pm 0.07$  %ID/g vs.  $2.57 \pm 0.49$  %ID/g at 4 h after injection). The pegylated RGD peptide showed higher renal accumulation at early time points ( $3.51 \pm 0.24$  %ID/g vs.  $2.18 \pm 0.23$  %ID/g at 30 min after injection) but more rapid clearance ( $1.82 \pm 0.29$  %ID/g vs.  $2.01 \pm 0.25$  %ID/g at 1 h after injection) than  $^{64}\text{Cu}$ -DOTA-RGD. The integrin receptor specificity of this radiotracer was demonstrated by blocking of tumor uptake by coinjection with nonradiolabeled c(RGDyK). The high tumor-to-organ ratios for the pegylated RGD peptide tracer (at 1 h after injection: tumor-to-blood ratio, 20; tumor-to-muscle ratio, 12; tumor-to-liver ratio, 2.7; and tumor-to-kidney ratio, 1.2) were confirmed by microPET and autoradiographic imaging in a subcutaneous U87MG tumor model. This tracer was also able to detect an orthotopic brain tumor in a model in which U87MG cells were implanted into the mouse forebrain. Although the magnitude of tumor uptake in the orthotopic xenograft was lower than that in the subcutaneous xenograft, the orthotopic tumor was still visualized with clear contrast from normal brain tissue. **Conclusion:** This study demonstrated the suitability of a PEG moiety for improving the in vivo kinetics of a  $^{64}\text{Cu}$ -RGD peptide tracer without compromising the tumor-targeting ability and specificity of the peptide. Systematic investigations of the effects of the size and geometry of PEG on tumor targeting and in vivo kinetics will lead to the development of radiotracers suitable for clinical applications such as visualizing and quantifying  $\alpha_v$ -integrin expression by PET. In addition, the same ligand labeled with therapeutic radionuclides may be applicable for integrin-targeted internal radiotherapy.

**Key Words:** molecular imaging; PET; radiopharmaceuticals; angiogenesis; integrin; Arg-Gly-Asp;  $^{64}\text{Cu}$ ; pegylation

**J Nucl Med 2004; 45:1776–1783**

---

**A**ngiogenesis, the formation and differentiation of blood vessels, plays a key role in tumor growth and metastasis spread and has become the new frontier for tumor control (1,2). Angiogenesis is a complex process involving extensive interplay among cells, soluble factors, and extracellular matrix components (3–11). Integrins are cell adhesion molecules known to be involved in multiple steps of angiogenesis and metastasis. The function of integrins during tumor angiogenesis has been studied most extensively for  $\alpha_v\beta_3$ -

---

Received Dec. 1, 2003; revision accepted Jun. 2, 2004.  
For correspondence or reprints contact: Peter S. Conti, MD, PhD, Department of Radiology, University of Southern California, 1510 San Pablo St., Suite 350, Los Angeles, CA 90033.  
E-mail: pconti@usc.edu

integrin and  $\alpha_v\beta_5$ -integrin, which are highly expressed on activated endothelial cells and tumor cells but not on quiescent vessels and normal cells (12). The expression of  $\alpha_v\beta_3$ -integrin is required for angiogenesis induced by fibroblast growth factor 2 and tumor necrosis factor  $\alpha$ , and the expression of  $\alpha_v\beta_5$ -integrin is required for angiogenesis induced by vascular endothelial growth factor and transforming growth factor  $\alpha$  (13). Monoclonal antibodies, peptides, and peptidomimetic antagonists of  $\alpha_v$ -integrins have been shown to block angiogenesis in both preclinical tumor models and phase I and II clinical trials by inhibiting endothelium-specific integrin survival signaling (14,15). The ability to noninvasively visualize and quantify the  $\alpha_v$ -integrin expression level during tumor growth and spread as well as during anti-integrin treatment will provide new opportunities to develop individualized therapeutic approaches, to select appropriate patients entering clinical trials for anti-integrin treatment, to establish optimized dosages and dose intervals for effective treatment on the basis of receptor occupancy studies, to detect early antiangiogenic responses and quantitatively evaluate treatment efficacy, and finally to cooptimize imaging and therapy via structure-activity studies.

Arg-Gly-Asp (RGD) peptide antagonists of  $\alpha_v$ -integrins have been labeled with different radionuclides for both imaging and therapeutic purposes. Notably, various investigators (16–20) labeled cyclic RGD peptides with  $^{18}\text{F}$  (half-life [ $t_{1/2}$ ], 119.7 min; 99%  $\beta^+$ ) for microPET imaging in various solid tumor models, and high tumor-to-background contrast was obtained. However, these radiotracers have some drawbacks: the labeling procedure is tedious and relatively inefficient, tumor uptake is modest, and tumor retention time is short. Although the tracers were able to localize  $\alpha_v$ -integrin-positive tumors, their utility in reflecting targeted radiotherapy is limited because no therapeutic fluorine isotope is available. Because of the existence of an imaging and therapy radionuclide pair ( $^{64}\text{Cu}/^{67}\text{Cu}$ ) for diagnosing and treating cancer,  $^{64}\text{Cu}$ -labeled RGD peptides with successful tumor-targeting properties will eventually be able to determine dosimetry and tumor responses to the same ligand labeled with therapeutic amounts of  $^{67}\text{Cu}$  for  $\alpha_v$ -integrin-mediated internal radiotherapy.

Chen et al. (21) recently described the synthesis of a  $^{64}\text{Cu}$ -labeled RGD peptide and microPET imaging of orthotopic MDA-MB-435 breast cancer tumor xenografts, with high tumor-to-contralateral background contrast. However, this tracer also had a rapid tumor washout rate and showed persistent activity accumulation in the liver and kidneys. The unfavorable in vivo pharmacokinetics of this tracer limit the application of a 1,4,7,10-tetraazacyclododecane- $N,N',N'',N'''$ -tetraacetic acid (DOTA)-RGD conjugate for tumor imaging and radiotherapy. Haubner et al. (22) chose to modify the RGD peptide with a glycosylate moiety to increase hydrophilicity and thus reduce blood clearance and reduce hepatobiliary excretion. We have found that poly-

ethylene glycol (PEG) is a suitable tool for modifying the RGD peptide, with improved in vivo kinetics.

Chen et al. (23) recently modified a cyclic RGD peptide, c(RGDyK), by introducing a monomethoxy PEG moiety (mPEG; molecular weight [MW], 2,000) into the lysine  $\epsilon$ -amino group. The resulting RGD-mPEG conjugate showed drastically decreased renal uptake and slightly increased liver accumulation compared with the parental RGD peptide. In this study, we inserted a heterobifunctional PEG linker (MW, 3,400) between DOTA and c(RGDyK). The resulting DOTA-PEG-RGD conjugate then was radiolabeled with  $^{64}\text{Cu}$  ( $t_{1/2}$ , 12.8 h; 19%  $\beta^+$ ) for microPET imaging studies with both subcutaneous and orthotopic U87MG glioblastoma models.

## MATERIALS AND METHODS

### Materials

c(RGDyK) was synthetically produced by solution cyclization of fully protected linear pentapeptide H-Gly-Asp(tert-butyloxy)-D-Tyr(tert-butyloxy)-Lys(butoxycarbonyl)-Arg(2,2,4,6,7-pentamethylidihydrobenzofuran-5-sulfonyl)-OH, followed by trifluoroacetic acid (TFA) deprotection in the presence of the free radical scavenger triisopropylsilane (23). RGD-PEG conjugate was prepared by coupling of c(RGDyK) with *t*-butoxycarbonyl (*t*-Boc)-protected PEG-succinimidyl ester (MW, 3,400), followed by TFA cleavage (24).  $^{64}\text{Cu}$  was produced on a CS-15 biomedical cyclotron at the School of Medicine, Washington University, by the  $^{64}\text{Ni}(p,n)^{64}\text{Cu}$  nuclear reaction (25). All reagents, unless otherwise specified, were of analytic grade and were commercially available. DOTA was purchased from MacroCyclics, Inc. *N*-Hydroxysulfosuccinimide (SNHS), 1-ethyl-3-[3-(dimethylamino)-propyl]carbodiimide (EDC), and Chelex 100 (50–100 mesh) were obtained from Aldrich.

Chromalux HB microplates were obtained from Dynex Technologies.  $^{125}\text{I}$ -Echistatin, labeled by the lactoperoxidase method to a specific activity of 74,000 GBq/mmol (2,000 Ci/mmol), was obtained from Amersham Biosciences. Echistatin was purchased from Sigma. Purified human  $\alpha_v\beta_3$ -integrin in a Triton X-100 formulation was obtained from Chemicon International.

Semipreparative reversed-phase high-pressure liquid chromatography (HPLC) was accomplished by use of a Waters 515 chromatography system with a 486 tunable absorbance detector. Purification was performed with a Vydac 218TP510 protein and peptide column (5  $\mu\text{m}$ ; 250  $\times$  10 mm). The flow rate was 5 mL/min; the mobile phase was changed from 95% solvent A (0.1% TFA in water) and 5% solvent B (0.1% TFA in acetonitrile) (0–2 min) to 35% solvent A and 65% solvent B at 32 min. The analytic HPLC method was performed with the same gradient system but with a Vydac 218TP54 column (5  $\mu\text{m}$ ; 250  $\times$  4.6 mm) and a flow rate of 1 mL/min. The absorbance was monitored at 218 nm. Radio-thin-layer chromatography (TLC) was performed by use of MKC18F plates (Whatman), Bioscan System 200, and Winscan software (version 2.2; BioScan Inc.). Reversed-phase extraction  $\text{C}_{18}$  SepPak cartridges were obtained from Waters.

### Preparation of DOTA-PEG-RGD Conjugate

DOTA was activated in situ by EDC at a molar ratio for DOTA:EDC:SNHS of 10:5:4 (21). RGD-PEG conjugate (8 mg; 2  $\mu\text{mol}$ ) dissolved in 1,600  $\mu\text{L}$  of water (5 mg/mL) was cooled to

4°C and added to a DOTA-sulfosuccinimide ester (OSSu) reaction mixture (10 µmol; calculated on the basis of SNHS), and the pH was adjusted to 8.5 with 1N NaOH. The reaction mixture was incubated overnight at 4°C. DOTA-PEG-RGD conjugate was purified by semipreparative HPLC. The sample containing the RGD conjugate was collected, lyophilized, and dissolved in H<sub>2</sub>O at a concentration of 1 mg/mL for use in radiolabeling reactions.

### **<sup>64</sup>Cu Radiolabeling**

DOTA-PEG-RGD was labeled with <sup>64</sup>Cu by the addition of 37–185 MBq (1–5 mCi) of <sup>64</sup>Cu (5–25 µg of DOTA-PEG-RGD per 37 MBq of <sup>64</sup>Cu) in 0.1N sodium acetate (pH 5.5) buffer and 45 min of incubation at 50°C. The reaction was terminated by the addition of 5 µL of ethylenediaminetetraacetic acid solution (10 mmol/L). The radiochemical yield was determined by radio-TLC with MKC18F TLC plates as the stationary phase and methanol:10% sodium acetate (70:30) as the eluent. <sup>64</sup>Cu-DOTA-PEG-RGD was purified by use of a C<sub>18</sub> SepPak cartridge with 85% ethanol as the elution solvent. Radiochemical purity was determined by radio-TLC or radio-HPLC. The ethanol was evaporated, the activity was reconstituted with phosphate-buffered saline, and the sample was passed through a 0.22-µm Millipore filter into a sterile multidose vial for use in animal experiments.

### **Octanol–Water Partition Coefficient**

About 370 kBq of <sup>64</sup>Cu-DOTA-c(RGDyK) or <sup>64</sup>Cu-DOTA-PEG-c(RGDyK) in 500 µL of saline were added to 500 µL of octanol in an Eppendorf microcentrifuge tube (Brinkman). The 2 layers were mixed for 10 min at room temperature, the tube was centrifuged at 14,000 rpm for 5 min (model 5415C Eppendorf microcentrifuge; Brinkman), and the counts in 100-µL aliquots of both organic and inorganic layers were determined by use of a  $\gamma$ -counter (Packard). The experiment was repeated 3 times.

### **Solid-Phase Receptor-Binding Assay**

The standard assay was performed as described previously with modifications (26). Microtiter-2 96-well plates (Dynatech Laboratories, Inc.) were coated with  $\alpha_v\beta_3$ -integrin (500 ng/mL; 100 µL per well) in coating buffer (Tris-HCl [pH 7.4] at 25 mmol/L, NaCl at 150 mmol/L, CaCl<sub>2</sub> at 1 mmol/L, MgCl<sub>2</sub> at 0.5 mmol/L, and MnCl<sub>2</sub> at 1 mmol/L) for 16 h at 4°C. The wells then were blocked for 2 h with 200 µL of blocking buffer (coating buffer with 1% radioimmunoassay-grade bovine serum albumin). The plates then were washed twice with binding buffer (coating buffer with 0.1% bovine serum albumin) and incubated with <sup>125</sup>I-echistatin (0.06 nmol/L) in the presence of various concentrations of RGD peptide (0.1 nmol/L–5 µmol/L) at room temperature for 3 h. After incubation, the plates were washed 3 times with binding buffer, and the radioactivity was solubilized with 2N boiling NaOH and subjected to  $\gamma$ -counting. Nonspecific binding of <sup>125</sup>I-echistatin to  $\alpha_v\beta_3$ -integrin was determined in the presence of echistatin at 100 nmol/L. The 50% inhibitory concentrations were calculated by nonlinear regression analysis by use of the GraphPad Prism computer fitting program (GraphPad Software, Inc.). Each data point represents the average value for triplicate wells.

### **Biodistribution Studies**

Animal experiments were conducted under a protocol approved by the University of Southern California Institutional Animal Care and Use Committee. Female athymic nude mice (*nu/nu*) obtained from Harlan at 4–6 wk of age were injected subcutaneously in the right front leg with  $5 \times 10^6$  U87MG glioblastoma cells suspended

in 150 µL of Eagle's minimum essential medium. When the tumors reached 0.4–0.6 cm in diameter (14–18 d after implantation), the mice were used for biodistribution and microPET imaging experiments.

Details of the orthotopic (intracranial) xenotransplant model in *nu/nu* mice were described previously (27). In brief, 10<sup>5</sup> U87MG tumor cells in 1 µL of RPMI medium were injected through a 33-gauge injection needle over 10 min into the nude mouse (4–6 wk old) forebrain 1.5 mm lateral and 0.5 mm anterior to the bregma and at a depth of 2.5 mm by use of a continuous infusion pump. The needle was removed, the burr hole was closed with bone wax, and the skin incision was closed with dermal glue. Mice were kept under ketamine–xylazine anesthesia during the procedure. This tumor cell number resulted in the growth of tumors in all experimental animals and a highly reproducible growth rate. At 5 wk after injection, when the tumors reached 3 mm or more in diameter, the mice were used for microPET imaging studies.

Nude mice bearing subcutaneously xenografted human U87MG glioblastoma tumors were injected intravenously with approximately 370 kBq (10 µCi) of <sup>64</sup>Cu-DOTA-PEG-RGD. Animals were euthanized at 30 min, 1 h, 2 h, and 4 h after injection. Blood, tumors, and major organs and tissues were collected and wet weighed, and counts were determined by use of a  $\gamma$ -counter. The percentage injected dose per gram (%ID/g) was determined for each sample. For each mouse, the radioactivity in the tissue samples was calibrated against a known quantity of the injected compound. Values are reported as mean  $\pm$  SD for groups of 4 animals. The receptor-mediated localization of the radiotracer was investigated by injection of <sup>64</sup>Cu-DOTA-PEG-RGD with c(RGDyK) at 10 mg/kg in a subcutaneous U87MG tumor model. Biodistributions were determined as described above at 1 h after injection for 4 mice per group.

### **microPET Imaging**

PET was performed by use of a microPET R4 rodent model scanner (Concorde Microsystems Inc.). The scanner has a computer-controlled bed and 10.8-cm transaxial and 8-cm axial fields of view. It has no septa and operates exclusively in the 3-dimensional list mode. All raw data were first sorted into 3-dimensional sinograms; this step was followed by Fourier rebinning and 2-dimensional (2D) filtered backprojection image reconstruction by use of a ramp filter with the Nyquist limit (0.5 cycle per voxel) as the cutoff frequency. For the subcutaneous tumor model, each mouse was injected with 14.8 MBq (400 µCi) of <sup>64</sup>Cu-DOTA-PEG-RGD via the tail vein, sacrificed at 1 h after injection by cervical dislocation under ketamine–xylazine anesthesia, and placed near the center of the field of view of the microPET scanner, where the highest image resolution and sensitivity are available. The mouse was scanned for 20 min and then subjected to whole-body autoradiography. The raw data were framed into one static frame without attenuation correction. For the orthotopic U87MG tumor model, a 20-min static image was obtained at 1 h after injection. The brain tumor was excised postmortem, fixed in buffered formalin, and embedded in paraffin for hexatoxylin–eosin staining.

### **Autoradiography**

Autoradiography was performed by use of a Packard Cyclone Storage Phosphor Screen system and a Bright 5030/WD/MR cryomicrotome (Hacker Instruments). Immediately after microPET scanning, the sacrificed mice with subcutaneous U87MG tumors were frozen in a dry ice–isopropyl alcohol bath for 2 min. The

bodies then were embedded in 4% carboxymethylcellulose (Aldrich) in water by use of a stainless steel mold. The mold was placed in the dry ice–isopropyl alcohol bath for 5 min and then into a  $-20^{\circ}\text{C}$  freezer for 1 h. The walls of the mold were removed, and the frozen block was mounted in the cryomicrotome. The block was cut into sections of  $50\ \mu\text{m}$ , and the desired sections were digitally photographed and captured for autoradiography. The sections were transferred into a chilled film cassette containing a Packard Super Resolution Screen (spatial resolution,  $0.1\ \text{mm}$ ) and kept there overnight at  $-20^{\circ}\text{C}$ . Screens were laser scanned by use of the Packard Cyclone system.

### Statistical Analysis

The data were expressed as mean  $\pm$  SD. A 1-way ANOVA was used for statistical evaluation. Means were compared by use of the Student *t* test. A *P* value of  $<0.05$  was considered significant.

## RESULTS

### DOTA Conjugation and $^{64}\text{Cu}$ Labeling

The synthesis of PEG-RGD may be performed by coupling of *t*-Boc-NH-PEG-CO<sub>2</sub>Su (MW, 3,400) with c(RGDyK), followed by TFA cleavage to unblock the *t*-Boc protecting group (24). A DOTA-PEG-RGD conjugate (Fig. 1) was produced in the presence of an excess amount of DOTA-OSSu activated in situ. The MW of the DOTA conjugate, evaluated by matrix-assisted laser desorption ionization–time-of-flight mass spectrometry, increased from 4,000 to 4,400. The mass spectrometry peak was broad (spectrum not shown) because of the polydispersity of PEG (28). The increase in MW, of approximately 400, corresponds to the conjugation of the macrocyclic chelator DOTA and is accompanied by the disappearance of amino group reactivity, demonstrated by the 6-trinitrobenzene sulfonic acid reaction (28). Contemporaneously, a slight change in the retention time (from 21.9 min for PEG-RGD to 21.5 min for DOTA-PEG-RGD) and a sharpening of the peak in reversed-phase HPLC elution were found.  $^{64}\text{Cu}$ -DOTA-PEG-RGD was prepared at radiochemical purities of about 50%, 80%, 95%, and  $\geq 98\%$  when 5, 10, 15, and 20  $\mu\text{g}$  of peptide per 37 MBq of  $^{64}\text{Cu}$  were used. The specific activity of  $^{64}\text{Cu}$ -DOTA-PEG-RGD ranged from 14,800 to 29,600 GBq/mmol (400–800 Ci/mmol).

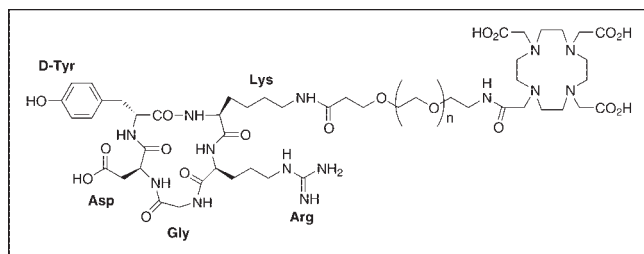


**FIGURE 1.** Schematic structure of DOTA-PEG-RGD. Hetero-functional PEG (MW, 3,400) is linked to the DOTA carboxylate group through the N terminus and to the lysine side chain  $\epsilon$ -amino group of c(RGDyK) through the C terminus.

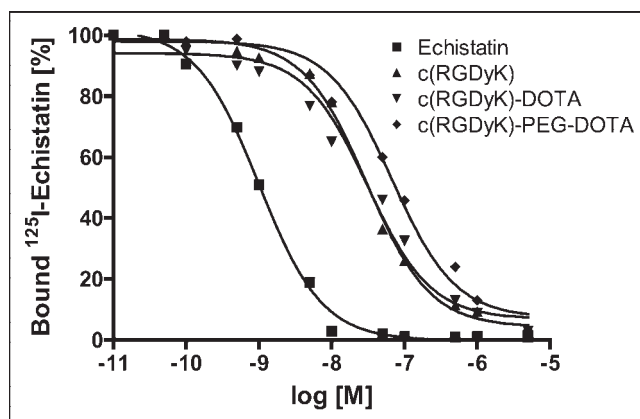


**FIGURE 2.** Competition between  $^{125}\text{I}$ -echistatin and unlabeled echistatin, c(RGDyK), c(RGDyK)-DOTA, and DOTA-PEG-c(RGDyK) for specific binding to purified  $\alpha_v\beta_3$ -integrin, as determined by a solid-phase receptor assay. All measurements were made in triplicate. M = molar concentration.

### Competitive Displacement and Hydrophilicity Studies

To compare the affinities of c(RGDyK)-DOTA and c(RGDyK)-PEG-DOTA for  $\alpha_v\beta_3$ -integrin, a competitive displacement study was performed (Fig. 2). The binding of  $^{125}\text{I}$ -echistatin to  $\alpha_v\beta_3$ -integrin was competed for by cold echistatin, c(RGDyK), c(RGDyK)-DOTA, and c(RGDyK)-PEG-DOTA in a concentration-dependent manner. All of the peptides were able to fully suppress the binding of the radioligand to purified human  $\alpha_v\beta_3$ -integrin. The concentrations required for half-maximal competition (50% inhibitory concentrations) were calculated to be  $1.01 \pm 0.23\ \text{nmol/L}$  for echistatin,  $30.3 \pm 5.8\ \text{nmol/L}$  for c(RGDyK),  $31.2 \pm 7.4\ \text{nmol/L}$  for c(RGDyK)-DOTA, and  $67.5 \pm 10.5\ \text{nmol/L}$  for c(RGDyK)-PEG-DOTA. Both the lead compound c(RGDyK)-DOTA and the pegylated analog c(RGDyK)-PEG-DOTA showed high hydrophilicity, as indicated from octanol–water partition coefficient measurements. LogP values for c(RGDyK)-DOTA and c(RGDyK)-PEG-DOTA were  $-2.8 \pm 0.04$  and  $-2.97 \pm 0.30$ , respectively.

### Biodistributions of $^{64}\text{Cu}$ -DOTA-PEG-RGD

The distributions of radioactivity in selected mouse organs and U87MG glioblastoma xenografts at various times after the administration of  $^{64}\text{Cu}$ -DOTA-PEG-RGD are shown in Figure 3. The radiotracer exhibited a rapid decrease in radioactivity over time in blood and most organs. At early time points, the high kidney activity was evidently attributable to the elimination of radiolabeled peptide in the urine. Analogously, radioactivity accumulated in the liver could have been caused by the radioactivity remaining in the blood as well as by partial bile excretion of the agent. The highest tumor uptake of  $^{64}\text{Cu}$ -DOTA-PEG-RGD ( $2.74 \pm 0.45\ \% \text{ID/g}$ ) was found at 30 min after injection and decreased to  $1.62 \pm 0.18\ \% \text{ID/g}$  at 4 h after injection, suggesting that the  $^{64}\text{Cu}$  was present in the tumor up to at least 4 h after injection.

A comparison of the kinetics of excretion of  $^{64}\text{Cu}$ -DOTA-PEG-RGD and  $^{64}\text{Cu}$ -DOTA-RGD in the blood, liver, kid-

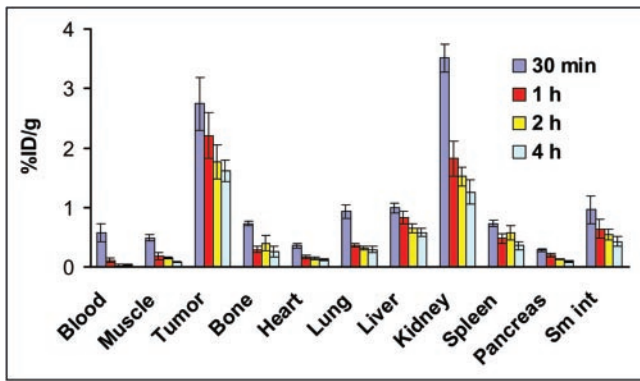


**FIGURE 3.** Biodistributions of  $^{64}\text{Cu}$ -DOTA-PEG-RGD in nude mice bearing subcutaneously xenotransplanted U87MG tumors. The data are reported as mean  $\pm$  SD ( $n = 4$ ). Sm int = small intestine.

neys, small intestine, and U87MG tumors is shown in Figure 4. The blood activity of  $^{64}\text{Cu}$ -DOTA-PEG-RGD ( $0.57 \pm 0.15$  %ID/g) was significantly higher than that of  $^{64}\text{Cu}$ -DOTA-RGD ( $0.35 \pm 0.09$  %ID/g) at 30 min after injection. The pegylated RGD peptide showed more rapid blood clearance than  $^{64}\text{Cu}$ -DOTA-RGD, as the blood activity was as low as  $0.02 \pm 0.02$  %ID/g at 2 h after injection for  $^{64}\text{Cu}$ -DOTA-PEG-RGD; the blood activity for  $^{64}\text{Cu}$ -DOTA-RGD was  $0.20 \pm 0.03$  %ID/g at 2 h after injection and remained unchanged at 4 h after injection. The kidney uptake of  $^{64}\text{Cu}$ -DOTA-PEG-RGD was higher than that of  $^{64}\text{Cu}$ -DOTA-RGD at early time points, although the pegy-

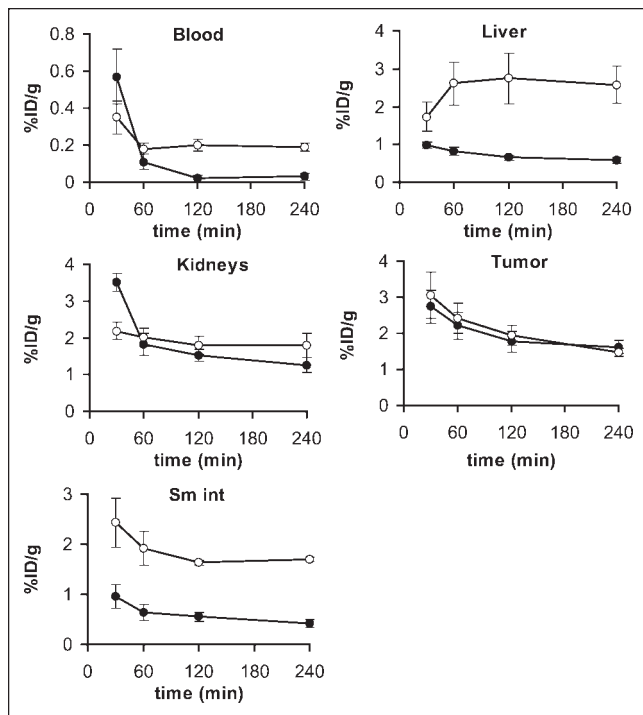


**FIGURE 4.** Comparison of biodistributions of  $^{64}\text{Cu}$ -DOTA-PEG-RGD (●) and  $^{64}\text{Cu}$ -DOTA-RGD (○) in nude mice. Error bars denote SDs ( $n = 4$ ). Sm int = small intestine.

lated RGD peptide showed more rapid renal clearance, resulting in significantly lower kidney activity accumulation at 4 h. The liver uptake of the pegylated RGD peptide was significantly lower than that of  $^{64}\text{Cu}$ -DOTA-RGD at all time points. Although the liver uptake of  $^{64}\text{Cu}$ -DOTA-RGD increased over time ( $2.57 \pm 0.49$  %ID/g at 4 h after injection),  $^{64}\text{Cu}$ -DOTA-PEG-RGD liver uptake decreased over time ( $0.58 \pm 0.07$  %ID/g at 4 h after injection). Intestinal activity accumulation of the pegylated RGD peptide was significantly higher than that of the lead compound at all time points ( $P < 0.001$ ). Pegylation had a minimal effect on tumor uptake and clearance.

Coinjection of c(RGDyK) (10 mg/kg) with  $^{64}\text{Cu}$ -DOTA-PEG-RGD resulted in a significant decrease in radioactivity in all dissected tissues, except the kidneys (Fig. 5). Uptake in tumors was reduced most dramatically, from  $2.21 \pm 0.38$  %ID/g to  $0.22 \pm 0.03$  %ID/g. The blocking experiment showed that the uptake and retention of  $^{64}\text{Cu}$ -DOTA-PEG-RGD were receptor dependent in tumors as well as several normal organs, such as the liver, spleen, and lungs.

#### microPET Imaging and Whole-Body Autoradiography

A 2D projection of the microPET image (20-min static single frame) of a female athymic nude mouse bearing an U87MG tumor on the right shoulder at 60 min after intravenous injection of 14.8 MBq (400  $\mu\text{Ci}$ ) of  $^{64}\text{Cu}$ -DOTA-PEG-RGD is shown in Figure 6A. The tumor was clearly visible, with high contrast relative to the contralateral background. Prominent uptake was also observed in the kidneys, intestinal tract, and urinary bladder; these data agreed well with the data obtained from direct tissue sampling. No activity accumulation was observed in the normal brain, probably because of the presence of an intact blood-brain barrier and a low level of  $\alpha_v$ -integrin expression.

Quantitation of tumor and major organ activity accumulation in microPET scanning was realized by measuring regions of interest that encompassed the entire organ in the

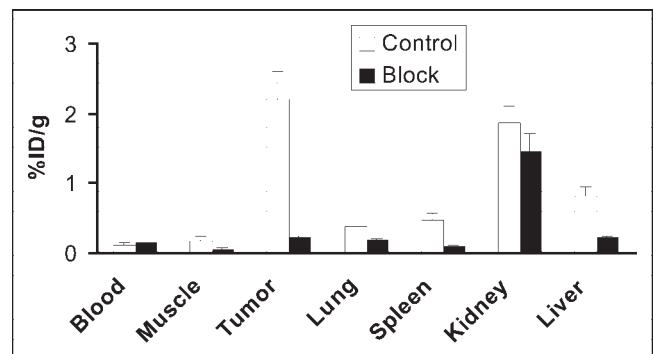


**FIGURE 5.** Biodistributions of  $^{64}\text{Cu}$ -DOTA-PEG-RGD in the absence and in the presence of c(RGDyK) at 1 h after injection in athymic nude mice with subcutaneous U87MG glioblastoma tumors. Reduced uptake in tumor, liver, muscle, and spleen in the blocking experiment indicated  $\alpha_v$ -integrin-mediated localization of  $^{64}\text{Cu}$ -DOTA-PEG-RGD in these tissues. Error bars denote SDs ( $n = 4$ ). Data are mean  $\pm$  SD ( $n = 4$ ).

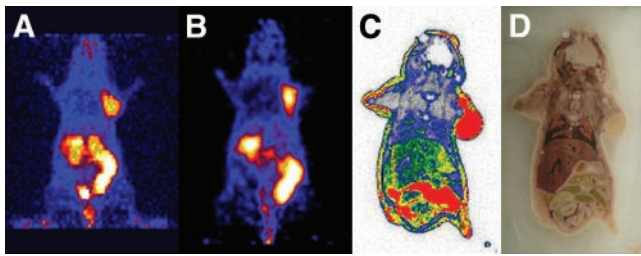


**FIGURE 6.** (A) 2D projection of U87MG tumor-bearing mouse at 60 min after injection of 14.8 MBq (400  $\mu$ Ci) of  $^{64}\text{Cu}$ -DOTA-PEG-RGD (20-min static image). (B) Coronal image of the same tumor-bearing mouse. (C) Digital autoradiograph of the section containing the tumor after microPET imaging. (D) Anatomic photograph of the section.

coronal orientation. Uptake in U87MG tumors, liver, and kidneys was calculated to be  $2.6 \pm 0.6$ ,  $0.8 \pm 0.2$ , and  $2.4 \pm 0.5$  %ID/g, respectively. These data were in good accordance with the biodistribution data obtained at 1 h after injection. To demonstrate that the uptake detected by microPET scanning of a living mouse corresponded to  $^{64}\text{Cu}$ -DOTA-PEG-RGD that had localized appropriately to an integrin-positive tumor after microPET scanning, the mouse was subjected to digital whole-body autoradiography. A comparison of the microPET image encompassing the U87MG tumor xenograft (Fig. 6B) and the corresponding autoradiographic section (Fig. 6C) clearly demonstrated the correlation between the regions of high uptake observed in the scan and autoradiographically detected tumor-associated radioactivity.

microPET imaging was also successful in visualizing an orthotopic U87MG glioblastoma implanted into the mouse forebrain (Fig. 7). Although the absolute tumor uptake ( $0.4 \pm 0.1$  %ID/g) was significantly lower than that of the subcutaneous tumor, the tumor-to-brain ratio still reached  $4.0 \pm 0.5$  because of the extremely low background activity accumulation in the normal brain tissue. Histologic staining of the mouse brain (Fig. 8) removed at the end of the scan confirmed the presence and location of the U87MG tumor, which measured  $2.9 \times 2.8$  mm.

## DISCUSSION

This study demonstrated that pegylation improves the in vivo kinetics of  $^{64}\text{Cu}$ -labeled RGD peptide and that  $^{64}\text{Cu}$ -

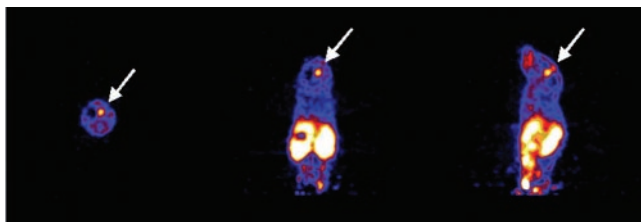


**FIGURE 7.** Transaxial, coronal, and sagittal slices (from left to right) of a mouse containing an orthotopically implanted U87MG tumor (arrows). The tumor is about 3 mm in diameter; the tumor-to-brain ratio is  $4.0 \pm 0.5$ .

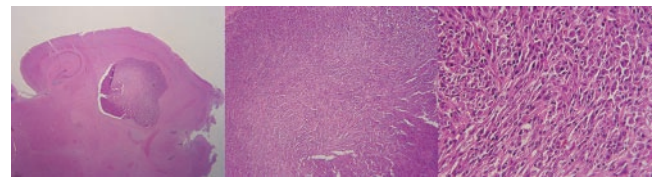


**FIGURE 8.** Histopathologic analysis of orthotopically injected U87MG brain tumor cells after microPET imaging. From left to right, panels show original, 4 $\times$ , and 20 $\times$  magnification. Tumor size and density of tumor cells were in accordance with volumetric and uptake information obtained from microPET scanning.

labeled pegylated RGD peptide is able to image a subcutaneous U87MG tumor xenograft and to visualize an orthotopic brain tumor implanted into the mouse forebrain by microPET scanning.

The overexpression of  $\alpha_v$ -integrins ( $\alpha_v\beta_3$  and  $\alpha_v\beta_5$ ) on solid tumor cells and activated endothelial cells has aroused interest in the development of radiolabeled RGD peptides for imaging and therapy of cancer. Various investigators have shown that  $^{18}\text{F}$ -labeled RGD peptides can accumulate in different tumors, such as breast cancer (16,20), brain tumor (17,23), and melanoma and osteosarcoma (18,19). However, the introduction of a prosthetic 4- $^{18}\text{F}$ -fluorobenzoyl group to the lysine side chain  $\epsilon$ -amino group resulted in unfavorable hepatobiliary excretion, as indicated by high uptake in the gallbladder and intestines; this situation may hamper the imaging of tumor lesions located in the lower abdomen and limit the activity dose that can be administered safely because of whole-body radiation exposure. Haubner et al. demonstrated that substituting a hydrophilic sugar moiety for the lysine resulted in predominant renal clearance for both  $^{125}\text{I}$ -labeled (22) and  $^{18}\text{F}$ -labeled (18,19) glycosylated RGD peptides. On the other hand, we found that the tumor-targeting ability and in vivo kinetics of an RGD peptide could be substantially improved by introducing a PEG moiety into the lysine side chain amino group. We coupled a c(RGDyK) peptide with mPEG (MW, 2,000) and labeled the c(RGDyK)-mPEG conjugate with  $^{125}\text{I}$ . The pegylated RGD peptide resulted in faster blood clearance and lower kidney uptake, without compromising the receptor-targeting ability, than c(RGDyK) (23). We also found that  $^{18}\text{F}$ -labeled pegylated RGD (PEG MW, 3,400) resulted in a longer tumor retention time and far less hepatobiliary excretion than the corresponding  $^{18}\text{F}$ -labeled RGD (24).

Because no therapeutic fluorine isotope is available,  $^{18}\text{F}$ -labeled RGD peptides will not be able to provide direct dosimetry information for integrin-targeted internal radiotherapy.  $^{64}\text{Cu}$  with 19% positron emission and 40%  $\beta$ -emission (maximum energy, 578 keV) efficiencies has the potential for both PET and therapy. Chen et al. previously conjugated c(RGDyK) with macrocyclic chelator DOTA and labeled the DOTA-RGD conjugate with  $^{64}\text{Cu}$  for PET of breast cancer tumors (21). This tracer showed significant liver uptake. Recent metabolic studies of  $^{111}\text{In}$ -diethylene-triaminepentaacetic acid (DTPA)-conjugated polypeptides

indicated that when DTPA was attached to the lysine of the polypeptides, a  $^{111}\text{In}$ -DTPA adduct of lysine was generated as the final radiometabolite after lysosomal proteolysis of the parental peptides in the liver (29). We assume that the prominent liver retention after intravenous administration of  $^{64}\text{Cu}$ -DOTA-RGD seen here may be ascribed to the combined effects of the transchelation of  $^{64}\text{Cu}$  from DOTA to superoxide dismutase (30) in the liver and the persistent localization of the final radiometal metabolite  $^{64}\text{Cu}$ -DOTA-lysine within the tissue. Therefore, the practical use of  $^{64}\text{Cu}$  as an imaging and therapeutic isotope relies on the development of new chelating agents for Cu(II) that have greater kinetic stability as well as on the prevention of the delivery of negatively charged metabolites to liver nonparenchymal cells via scavenger receptor-mediated endocytosis (31).

Intrigued by the ability of pegylation to improve the tumor-targeting and in vivo kinetics of both  $^{125}\text{I}$ - and  $^{18}\text{F}$ -labeled RGD peptides, we extended our study to observe the impact of pegylation on  $^{64}\text{Cu}$ -DOTA-RGD. The results of an isolated, immobilized integrin receptor-binding assay indicated that introduction of the PEG moiety at the lysine side chain amino group had a modest influence on  $\alpha_v\beta_3$ -integrin affinity and selectivity. All of the RGD peptide ligands bound  $\alpha_v\beta_3$ -integrin with a significantly lower affinity than echistatin, which is folded in a series of irregular loops to form a rigid core stabilized by 4 disulfide bridges (32). It is also worth noting that the introduction of a PEG moiety with an MW of 3,400 significantly reduced the circulatory  $t_{1/2}$  of the pegylated radiotracer, in contrast to the results reported for many other pegylated proteins and polypeptides (33). Since the octanol–water partition coefficients of the cyclic RGD peptide and pegylated RGD peptide tracers were similar, the more rapid blood clearance of the pegylated RGD peptide could have been attributable to the fact that this compound showed reduced interactions with blood elements (plasma proteins or blood cells) rather than changes in hydrophilicity on modification.

Both  $^{64}\text{Cu}$ -DOTA-RGD and  $^{64}\text{Cu}$ -DOTA-PEG-RGD were cleared rapidly from the kidneys. In general, PEG shows little toxicity and is eliminated from the body intact either by the kidneys (for PEG of  $<30$  kDa) or in the feces (for PEG of  $>20$  kDa) (34–36); subsequent reabsorption occurs in the proximal tubular cells, where the pegylated peptide is internalized and degraded in the lysosomes. Following this pathway, the main radiolabeled catabolite of  $^{64}\text{Cu}$ -DOTA-PEG-RGD probably is  $^{64}\text{Cu}$ -DOTA-PEG-Lys.  $^{64}\text{Cu}$ -DOTA-Lys and  $^{64}\text{Cu}$ -DOTA-PEG-Lys have the same overall negative charge ( $-1$ ), but  $^{64}\text{Cu}$ -DOTA-PEG-RGD had significantly lower liver uptake and more rapid liver clearance. We assume that the PEG polymer, along with the associated water molecules, acts like a shield to wrap the  $^{64}\text{Cu}$ -DOTA chelate and reduces the apparent negative charge, and the negative charge density thus reduces the apparent affinity of the radiometal metabolite for hepatic scavenger receptors. This notion agrees with the phenome-

non in which an increase in the negative charge density of proteins by acylation efficiently increases liver uptake (37).

The features of rapid blood and renal clearance and limited hepatic and biliary excretion permit high signal-to-noise ratios for in vivo imaging soon after injection (1 h). The activities quantified in the mouse tumor, liver, and kidneys were comparable to those obtained by the direct tissue sampling technique. microPET imaging used with the orthotopic U87MG tumor model revealed a good tumor-to-brain ratio; the magnitude of uptake of the orthotopic tumor was about 5 or 6 times lower than that of the subcutaneous tumor. Whether the blood–brain barrier or different integrin expression characteristics of orthotopic brain tumors and subcutaneous tumors are responsible for this difference in uptake needs to be investigated further.

The receptor specificity of the RGD peptide was not significantly affected by the introduction of a PEG moiety and a  $^{64}\text{Cu}$ -DOTA radiolabel, because of the invariance of the “kinked” conformation of the pentapeptide (38). The unaltered tumor uptake and clearance and the favorable biokinetics make this radiopharmaceutical suitable for PET of solid tumors that overexpress  $\alpha_v$ -integrin and for integrin-targeted internal radiotherapy when therapeutic amounts of  $^{64}\text{Cu}$ - or  $^{67}\text{Cu}$ -labeled pegylated RGD peptide are applied. A radionuclide with PET and therapeutic capacities, such as  $^{64}\text{Cu}$ , could be very advantageous, because accurate individualized dosimetry could be obtained for each patient with PET before radiotherapy. The DOTA-PEG-RGD conjugate could also be used with  $^{86}\text{Y}$  ( $t_{1/2}$ , 14.7 h; 33%  $\beta^+$ ) as a surrogate marker to detect the uptake and dosimetry of  $^{90}\text{Y}$ -labeled RGD.

We recognize that 2 important issues remain unresolved. The first issue is whether the magnitude of tumor uptake obtained from PET correlates well with the tumor integrin expression level. The ability to measure tumor integrin receptor density noninvasively could have great value in predicting the effectiveness of RGD peptide therapy in patients with brain tumors and other solid tumors that express  $\alpha_v$ -integrins. Our recent quantitative analysis of tracer kinetics with the reference tissue sampling technique, which assumes that the radiolabel is not irreversibly trapped within the reference region and that the rate of turnover of the exchanging spaces in both the tumor and the reference tissue is rapid compared with the duration of the time–activity curves (X. Chen, P.S. Conti, unpublished data, 2003), has suggested the feasibility of this reference method (39) for quantifying  $\alpha_v$ -integrin receptor density during tumor growth and in response to competition from a nonlabeled RGD peptide or anti-integrin drugs targeted to  $\alpha_v$ -integrins. Our future studies will focus on the validation of the results of such an analysis with traditional Western blots and in vitro receptor autoradiography.

The second issue is whether the tumor retention of a suitably labeled RGD peptide is attributable to interactions with  $\alpha_v$ -integrins expressed on the neovasculature, on the tumor cells, or on a combination of both cell types. The intrinsic resolution of PET will not allow this question to be

answered directly. In this regard, it is possible that further advances in molecular biology may elucidate subclasses of  $\alpha_v$ -integrins present on endothelial cells versus tumor cells, thereby providing an approach for developing more specific diagnostic and therapeutic ligands in the future. In the interim, existing agents may be used to assess overall  $\alpha_v$ -integrin activity in tumors.

## CONCLUSION

A  $^{64}\text{Cu}$ -labeled pegylated RGD peptide was developed for PET imaging of tumor  $\alpha_v$ -integrin expression. This new radiotracer was directly compared with  $^{64}\text{Cu}$ -DOTA-RGD in vivo, and the results suggested that DOTA-PEG-RGD is a suitable ligand for labeling radiometals that can form stable complexes with the DOTA moiety for both imaging and therapeutic applications. Optimization of this tracer by systematic investigation of the impact of PEG size and geometry and the application of different RGD peptide and peptidomimetic antagonists of  $\alpha_v$ -integrins and different chelating agents for Cu(II) may further improve the imaging and therapeutic potentials of the peptides.

## ACKNOWLEDGMENTS

This work was performed in part with contributions from National Institute of Biomedical Imaging and Bioengineering grant R21 EB001785, American Chemical Society grant ACS-IRG-580007-42, the Wright Foundation, Department of Defense (DOD) Breast Cancer Research Program (BCRP) Concept Award DAMD17-03-1-0752, DOD BCRP Idea Award BC030012, and National Cancer Institute (NCI) grant P20 CA86532.  $^{64}\text{Cu}$  was provided by Washington University Medical School with partial funding from NCI grant R24 CA86307.

## REFERENCES

- Folkman J. Role of angiogenesis in tumor growth and metastasis. *Semin Oncol.* 2002;29(suppl 16):15–18.
- Brower V. Tumor angiogenesis: new drugs on the block. *Nat Biotechnol.* 1999; 17:963–968.
- Gasparini G. The rationale and future potential of angiogenesis inhibitors in neoplasia. *Drugs.* 1999;58:17–38.
- Choi KS, Bae MK, Jeong JW, Moon HE, Kim KW. Hypoxia-induced angiogenesis during carcinogenesis. *J Biochem Mol Biol.* 2003;36:120–127.
- Jain RK. Tumor angiogenesis and accessibility: role of vascular endothelial growth factor. *Semin Oncol.* 2002;29(suppl 16):3–9.
- Mignatti P, Rifkin DB. Plasminogen activators and matrix metalloproteinases in angiogenesis. *Enzyme Protein.* 1996;49:117–137.
- Thorgeirsson UP, Lindsay CK, Cottam DW, Gomez DE. Tumor invasion, proteolysis, and angiogenesis. *J Neurooncol.* 1994;18:89–103.
- Hood JD, Cheresch DA. Role of integrins in cell invasion and migration. *Nat Rev Cancer.* 2002;2:91–100.
- Kalluri R. Basement membranes: structure, assembly and role in tumor angiogenesis. *Nat Rev Cancer.* 2003;3:422–433.
- Yancopoulos GD, Davis S, Gale NW, Rudge JS, Wiegand SJ, Holash J. Vascular-specific growth factors and blood vessel formation. *Nature.* 2000;407:242–248.
- Vicari AP, Caux C. Chemokines in cancer. *Cytokine Growth Factor Rev.* 2002; 13:143–154.
- Eliceiri BP, Cheresch DA. The role of  $\alpha_v$  integrins during angiogenesis: insights into potential mechanisms of action and clinical development. *J Clin Investig.* 1999;103:1227–1230.
- Friedlander M, Brooks PC, Shaffer RW, Kincaid CM, Varner JA, Cheresch DA.

Definition of two angiogenic pathways by distinct  $\alpha_v$  integrins. *Science.* 1995; 270:1500–1502.

- Kumar CC. Integrin  $\alpha_v\beta_3$  as a therapeutic target for blocking tumor-induced angiogenesis. *Curr Drug Targets.* 2003;4:123–131.
- Kerr JS, Slee AM, Mousa SA. The  $\alpha_v$ -integrin antagonists as novel anticancer agents: an update. *Expert Opin Investig Drugs.* 2002;11:1765–1774.
- Chen X, Shahinian A, Park R, Bozorgzadeh MH, Bading JR, Conti PS.  $^{18}\text{F}$ -Labeled cyclic RGD peptide for PET imaging of tumor angiogenesis [abstract]. *J Nucl Med.* 2003;55(suppl 5):271P–272P.
- Chen X, Park R, Shahinian AH, et al.  $^{18}\text{F}$ -Labeled RGD peptide: initial evaluation for imaging brain tumor angiogenesis. *Nucl Med Biol.* 2004;31:179–189.
- Haubner R, Wester HJ, Weber WA, et al. Noninvasive imaging of  $\alpha_v\beta_3$  integrin expression using  $^{18}\text{F}$ -labeled RGD-containing glycopeptide and positron emission tomography. *Cancer Res.* 2001;61:1781–1785.
- Haubner R, Kuhast B, Mang C, et al. [ $^{18}\text{F}$ ]Galacto-RGD: synthesis, radiolabeling, metabolic stability, and radiation dose estimates. *Bioconjug Chem.* 2004;15:61–69.
- Ogawa M, Hatano K, Oishi S, et al. Direct electrophilic radiofluorination of a cyclic RGD peptide for in vivo  $\alpha_v\beta_3$  integrin related tumor imaging. *Nucl Med Biol.* 2003;30:1–9.
- Chen X, Park R, Tohme M, Shahinian AH, Bading JR, Conti PS. microPET and autoradiographic imaging of breast cancer  $\alpha_v$ -integrin expression using  $^{18}\text{F}$ - and  $^{64}\text{Cu}$ -labeled RGD peptide. *Bioconjug Chem.* 2004;15:41–49.
- Haubner R, Wester HJ, Burkhardt F, et al. Glycosylated RGD-containing peptides: tracer for tumor targeting and angiogenesis imaging with improved biokinetics. *J Nucl Med.* 2001;42:326–336.
- Chen X, Park R, Shahinian AH, Bading JR, Conti PS. Pharmacokinetics and tumor retention of  $^{125}\text{I}$ -labeled RGD peptide are improved by PEGylation. *Nucl Med Biol.* 2004;31:11–19.
- Chen X, Park R, Hou Y, et al. microPET imaging of brain tumor angiogenesis with  $^{18}\text{F}$ -labeled PEGylated RGD peptide. *Eur J Nucl Med Mol Imaging.* 2004; 31:1081–1089.
- McCarthy DW, Shefer RE, Klinkowstein RE, et al. Efficient production of high specific activity  $^{64}\text{Cu}$  using a biomedical cyclotron. *Nucl Med Biol.* 1997;24:35–43.
- Kumar CC, Nie H, Rogers CP, et al. Biochemical characterization of the binding of echistatin to integrin  $\alpha_v\beta_3$  receptor. *J Pharmacol Exp Ther.* 1997;283:843–853.
- MacDonald TJ, Taga T, Shimada H, et al. Preferential susceptibility of brain tumors to the antiangiogenic effects of an  $\alpha_v$ -integrin antagonist. *Neurosurgery.* 2001;48:151–157.
- Veronese FM, Saccà B, Polverino de Lauro P, et al. New PEGs for peptide and protein modification, suitable for identification of the PEGylation site. *Bioconjug Chem.* 2001;12:62–70.
- Franano FN, Edwards WB, Welch MJ, Duncan JR. Metabolism of receptor targeted  $^{111}\text{In}$ -DTPA-glycoproteins: identification of  $^{111}\text{In}$ -DTPA- $\epsilon$ -lysine as the primary metabolic and excretory product. *Nucl Med Biol.* 1994;21:1023–1034.
- Bass LA, Wang M, Welch MJ, Anderson CJ. In vivo transchelation of copper-64 from TETA-octreotide to superoxide dismutase in rat liver. *Bioconjug Chem.* 2000;11:527–532.
- Franssen EJ, Jansen RW, Vaalburg M, Meijer DK. Hepatic and intrahepatic targeting of an anti-inflammatory agent with human serum albumin and neoglycoproteins as carrier molecules. *Biochem Pharmacol.* 1993;45:1215–1226.
- Calvete JJ, Wang Y, Mann K, Schafer W, Niewiarowski S, Stewart GJ. The disulfide bridge pattern of snake venom disintegrins, flavridin and echistatin. *FEBS Lett.* 1992;309:316–320.
- Monfardini C, Veronese FM. Stabilization of substances in the circulation. *Bioconjug Chem.* 1998;9:418–450.
- Delgado C, Francis GE, Fisher D. The uses and properties of PEG-linked proteins. *Crit Rev Ther Drug Carrier Syst.* 1992;9:249–304.
- Behr TM, Sharkey RM, Sgouros G, et al. Overcoming the nephrotoxicity of radiometal-labeled immunoconjugates: improved cancer therapy administered to a nude mouse model in relation to the internal radiation dosimetry. *Cancer.* 1997;80(suppl 12):2591–2610.
- Yamaoka T, Tabata Y, Ikada Y. Distribution and tissue uptake of poly(ethylene glycol) with different molecular weights after intravenous administration to mice. *J Pharm Sci.* 1994;83:601–606.
- Yamasaki Y, Hisazumi J, Yamaoka K, Takakura Y. Efficient scavenger receptor-mediated hepatic targeting of proteins by introduction of negative charges on the proteins by aconylation: the influence of charge density and size of the protein molecules. *Eur J Pharm Sci.* 2003;18:305–312.
- Dechantsreiter MA, Planker E, Matha B, et al. N-Methylated cyclic RGD peptides as highly active and selective  $\alpha_v\beta_3$  integrin antagonists. *J Med Chem.* 1999;42:3033–3040.
- Patlak CS, Blasberg RG. Graphical evaluation of blood-to-brain transfer constants from multiple-time uptake data: generalizations. *J Cereb Blood Flow Metab.* 1985;5:584–590.